Study of Flowfield around Truncated Square Protuberance in Hypersonic Flow.

A.Ahmed, Ajmal Baig, S.Bilal, S.Zahir
N E S C O M
Islamabad
Pakistan

OVERVIEW:
The present CFD study is done on the effects of shock wave and boundary layer interactions and the resulting pressure distribution on the windward faces of a truncated square protuberance, at hypersonic speed of Mach no. 5.0. The CFD solver was run on four protuberances mounted on a flat plate. Model 1 is a simple truncated square protuberance of equal width and length and height of 2.2D, where D=2.5cm, is the width of the model. Model 2,3 and 4 are of the same dimensions but with relief angles of 30^o , 45^o and 60^o respectively. The models were mounted on a flat plate of dimensions $33x24cm^{2.}$ The distance between the leading edge of the plate and the protuberance was 16.75cm. Separate 3-D grids were developed for each model. The flow was initialized at Mach no. of 5.0 and stagnation pressure and temperature of 30bars and 400k. The solver model used was coupled implicit with second order discretization. Velocity gradient adaption was utilized to refine grid and improve results. The turbulent model used was 1-equation Spalart-Almaras. CFD results have been finally compared with experimental results.

1. NOMENCLATURE:

D=Width of protuberance (cm)
H=Height of protuberance (cm)
M= Freestream Mach number
P= Local Pressure (Pa)
Ps= Freestream static pressure (Pa)
P_0 = Freestream stagnation pressure (Pa)
T_0 = Freestream stagnation temperature (K)
x=Local distance along x-axis (cm)
y=Local distance along y-axis (cm)
z=Local distance along z-axis (cm)

2. HYPERSONIC FLOWS

Hypersonic flows have undergone extensive research recently and various different branches of this field have been studied and developed. Hypersonic flows with different interacting phenomena such as shock wave and shock/boundary layer induced separation is a very important field. Considerable study and research has undergone in this field . Most of the present work is related to the experimental study. However with the advent of CFD numerical simulations are also complimenting experimental results. Since experimentation of hypersonic flows with rectangular protuberance has already been done [ref 1] the present study is on slotted rectangular protuberances. The experimental results have been

done on simple rectangular shafts. By comparing these results by our own numerical solutions, we have further done additional work on a flow facing protuberance with slots of different angles of incidence to the flow. Hence pressure distributions on plate and protuberance have been plotted for each case.

3. MODEL GEOMETRY:

The model consists of a flat plate and a rectangular protuberance with square cross secton. The flat plate is set to the free-stream direction. The protuberance is mounted on the flat plate perpendicularly. The distance between the leading edge of the plate and protuberance is 16.75cm.
The geometrical characteristics of the model are:

- Area of flat plate: $33x24cm^2$
- Height of protuberance: H= 5.5cm
- Width of protuberance: D= 2.5cm
- Distance of leading edge of plate to protuberance base=16.75cm

Relief angles of models-2,-3 and -4 were 30^o , 45^o and 60^o respectively. The relief angles were generated from the windward face of the protuberance such that it would cut the top face at its centre.

4. GRID GENERATION:

There were three separate 3-D grids developed for the following case which are shown in FIG 1-4. Initially coarse grids were developed with 60, 25 and 30 nodes in x y and z directions respectively. The flow was initialized on the same grids. Later however velocity gradient adaption was employed to refine grids at required nodes.

5. FLOW CONDITIONS

P_0 =3.0e+06 Pa
T_0 =400 K
M = 5.0

6. SOLVER CONDITIONS

The solver used is Fluent6.2.03 which is a commercially available CFD software. The solution was run on the density-based scheme which is actually a coupled equation solver, since the flow is in hypersonic regime. The grid models were initially run on coarse mesh. When residuals were minimized the adaption techniques were employed. Adaption was done on velocity gradients whereby dynamic adaption ensured refinement at every 20 iterations. CFL was kept constant at 2.5.

7. GOVERNING EQUATION

A 3D coupled explicit model was used. The system of governing equations for a single-component fluid, written to describe the mean flow properties, is cast in integral Cartesian form for an arbitrary control volume **V** with differential surface area **dA** as follows:

$$\frac{\partial}{\partial \mathbf{t}} \int_{\mathbf{v}} \mathbf{W}.\mathbf{dV} \quad + \oint [\mathbf{F} - \mathbf{G}].\mathbf{dA} \quad = \int_{\mathbf{V}} \mathbf{H}.\mathbf{dV}$$

where the vectors **W,F**, and **G** are defined as :

$$W = \begin{Bmatrix} \rho \\ \rho u \\ \rho v \\ \rho w \\ \rho E \end{Bmatrix}, \quad F = \begin{Bmatrix} \rho v \\ \rho v u + p\hat{i} \\ \rho v + p\hat{j} \\ \rho v w + p\hat{k} \\ \rho v E + pv \end{Bmatrix},$$

$$G = \begin{Bmatrix} 0 \\ \tau_{xi} \\ \tau_{yi} \\ \tau_{zi} \\ \tau_{ij} v_j + q \end{Bmatrix}$$

and the vector H contains source terms such as body forces and energy sources. Here ρ, v, E, and **p** are the density, velocity, total energy per unit mass, and pressure of the fluid, respectively. τ is the viscous stress tensor, and **q** is the heat flux.

Total energy E is related to the total enthalpy H by

$$E = H - p/\rho$$

where

$$H = h + |v|^2/2$$

7.1. Turbulent Model

A single equation turbulent Spalart-Almaras was used. The transported variable in the Spalart-Almaras model, $\tilde{\nu}$, is identical to the turbulent kinematic viscosity except in the near-wall (viscous-affected) region. The transport equation for $\tilde{\nu}$ is

$$\frac{\partial}{\partial t}(\rho\tilde{\nu}) + \frac{\partial}{\partial x_i}(\rho\tilde{\nu}u_i) = G_\nu + \frac{1}{\sigma_{\tilde{\nu}}}\left[\frac{\partial}{\partial x_j}\left\{(\mu+\rho\tilde{\nu})\frac{\partial\tilde{\nu}}{\partial x_j}\right\} + C_{b2}\rho\left(\frac{\partial\tilde{\nu}}{\partial x_j}\right)^2\right] - Y_\nu + S_{\tilde{\nu}}$$

where $G\nu$ is the production of turbulent viscosity and Y_ν is the destruction of turbulent viscosity that occurs in the near-wall region due to wall blocking and viscous damping. $\sigma_{\tilde{\nu}}$ and C_{b2} are constants and ν is the molecular kinematic viscosity. S_ν is a user-defined source term.

8. RESULTS and DISCUSSION:

The CFD solver generated numerical solutions for the cases defined and finally the post-processed results were in the form of contour plots and distribution charts.

8.1. Flow visualization:

The schileren photograph of experimental results [ref 1] is shown in fig 5. The flow visualised for the same configuration is seen in fig 6 in the form of unfilled mach contours. It can be clearly seen from the Mach contours that boundary layer develops on the flat plate due to viscous effects and then boundary-layer separation occurs just as in fig 5. The labels given in both figures are as follows:

1. Bow Shock
2. Separated Shock
3. Triple Point

These three parameters are seen around the same location in both figures and overall both figures show close resemblance. The results are therefore in good qualitative concurrence.

Mach contours of models-2, -3 and -4 are shown in FIG 7-9 respectively.

8.2. Pressure distribution along flat plate:

The pressure distributions shown in FIG 10 & 11 are of pressure along the centerline of flat plate upstream of the protuberance.

Comparison between experimental and CFD results:

In FIG 10, a comparison is done between experimental results [ref 1] and CFD results of Model-1. It can be seen from the graph that both results show similar trends. However it can be seen that pressure starts increasing for experiment at

x/D= -5.5 while for CFD the same point occurs at x/D= -4.25. Both graphs then undergo a low peak to decline and then jump to reach high peaks. The low peak of experimental is at P/Ps=3.0 where x/D=-3.0 and high peak is at P/Ps=13.1 where x/D=-0.25. Similarly for CFD the low peak is P/Ps=3.8 where x/D=-2.0 and high is P/Ps=22.4 where x/D=-0.14. The difference in results is due to the limitations of solver at hypersonic speeds.

Comparison between CFD results of all the models:

In FIG 11, a comparison is done between CFD results of all the models. It can be clearly seen that the trends and values of all four models are almost same. The low peaks is same all four models at P/Ps=3.79 where x/D= -1.875. However the high peaks lie at slightly different locations which are given in TAB 1 below:

TAB 1: High peak values of CFD results

	X/D	P/Ps
Model-1	-0.14	22.4
Model-2	-0.12	22.1
Model-3	-0.137	23.1
Model-4	-0.146	24.0

8.3. Pressure distribution along windward face of protuberance

The pressure distributions shown in FIG 12 & 13 are of pressure along the centreline of windward face of protuberance. The pressure values are taken along the height of the protuberance.

Comparison between experimental and CFD results:

In FIG 12, a comparison is done between experimental results [ref 1] and CFD results of Model-1. It can be seen from the graph that both results show similar trends. The graphs follow a wavy pattern with a minimum peak near bottom and maximum peak near the mid-section. The minimum peak for experiment is at P/Ps=5.7 where y/D=0.28 while close to the CFD results for the same location at P/Ps=5.5 where y/D=0.35. Similarly the maximum peak for experimental study is at P/Ps=58.0 where y/D=1.6. The maximum peak for CFD is at P/Ps=55.4 where x/D=1.15. The difference in results is due to the limitations of solver at hypersonic speeds.

Comparison between CFD results of all the models:

In FIG 13, a comparison is done between CFD results of all the models. It can be clearly seen that the trend of the models except model-1 is same. In model-1, the graph follows a wavy pattern from bottom to top. However in rest of the models a sudden jump occurs near the location where relief angle starts. The location where jump occurs for each model corresponding to its relief angle start point is given in TAB 2 below:

TAB 2: Location where jump in pressure occurs for CFD results of truncated models.

	Jump in pressure along windward face		Relief Angle start point y/D
	P/Ps	y/D	
Model-2	29.9	1.38	1.334
Model-3	8.95	1.725	1.70
Model-4	1.95	1.96	1.92

It is also noted that for all models except model-2 the maximum peak is same. But for model-2 the maximum peak pressure is greater than the rest and it is because of the vicinity of a sharp bend of the relief angle.

9. CONCLUSION

9.1. The visualization of CFD solutions as Mach contours and schileren photographs of experimental study are very similar.

9.2. The pressure distribution along flat plate for upstream locations show similar trends. The peak location near the protuberance is higher for the CFD study as compared to experimental results. This is due to the limitations of solver at hypersonic speeds. Similarly pressure distributions along windward face of protuberance is same for experimental and CFD results. The maximum peak pressure is almost same however the locations are different.

9.3. The CFD study of different truncated protuberances clearly show that relief angles do not have any effect on boundary layer separation. However relief angles do have a significant effect on pressure distribution along windward face of protuberance. The relief angle cause a sudden jump in the pressure near relief angle start point.

REFERENCES:

[REF 1] "Flow field features on Hypersonic Flow over Rectangular Obstacles", by Li.Suxun, Chen. Yonkang and Ni.ZY, Journal of Visualization, Vol4, No.1(2001) 73-79

[REF2] "The Effects of Protuberances on Interactive Supersonic Flowfield through CD-Nozzle", by S.Zahir, A.Baig, Z.Ye, A.Ahmed, 24th AIAA Applied Aerodynamics Conference, AIAA-2006-3327

[REF 3] NASA report, "Solid Rocket Thrust Vector Control", NASA SP 8114.

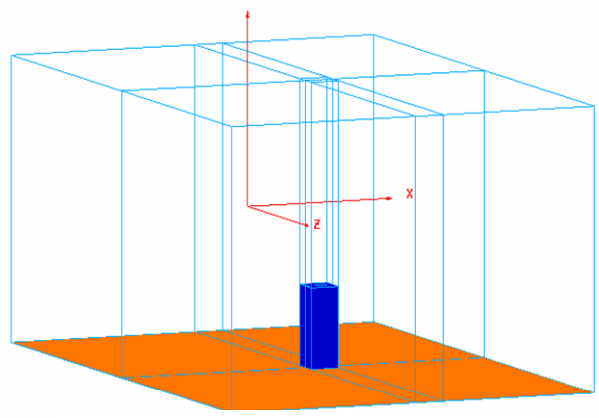

FIG 1: Grid for Simple protuberance without truncation mounted on flat plate (MODEL-1)

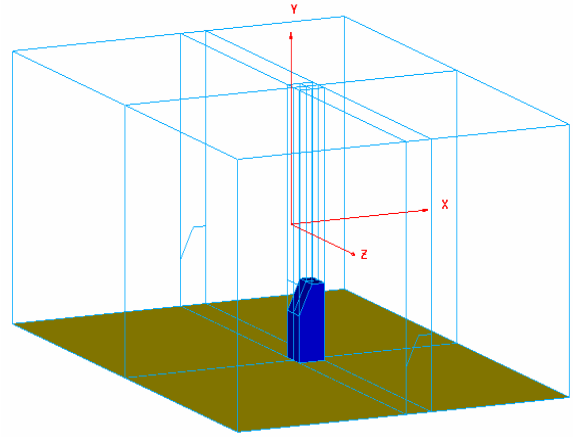

FIG 2: Grid for protuberance with 30° relief angle (MODEL-2)

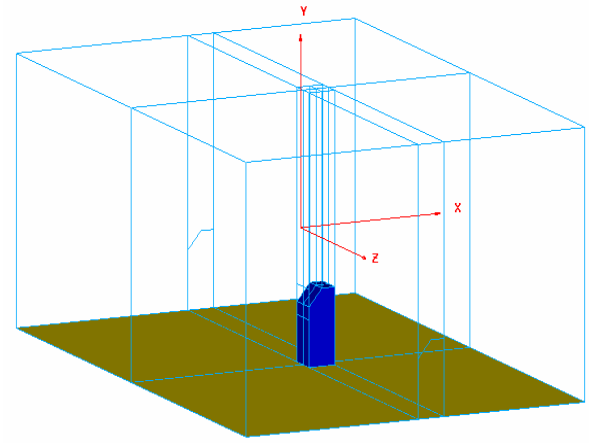

FIG 3: Grid for protuberance with 45° relief angle (MODEL-3)

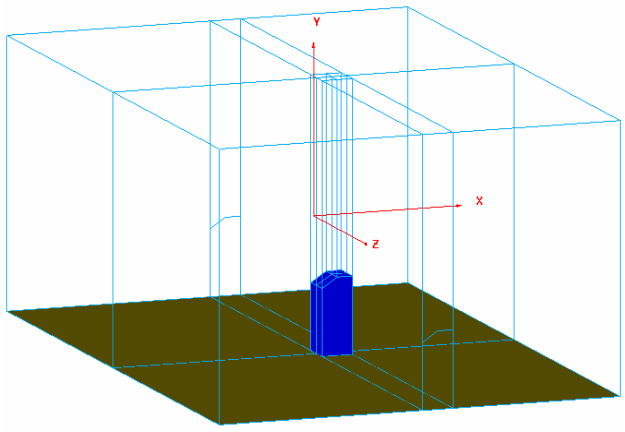

FIG 4: Grid for protuberance with 60 deg relief angle (MODEL-4)

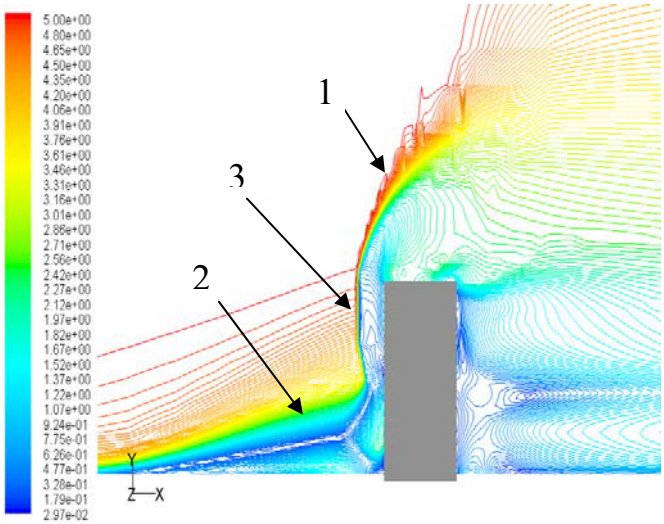

FIG 6: Flow visualised for CFD results as Mach contours

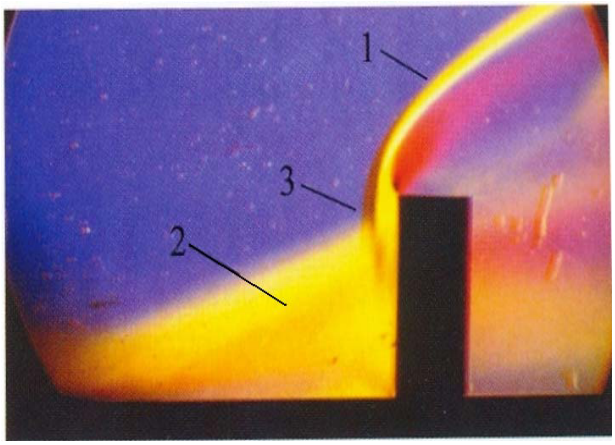

FIG 5: Schileren photo for experimental results [ref 1]

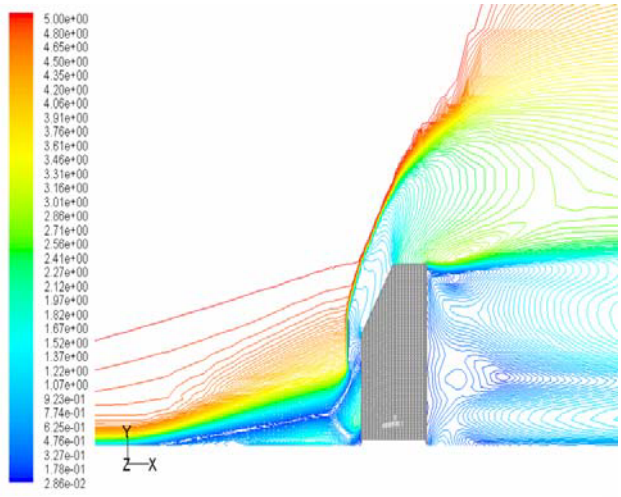

FIG 7: Mach contours for protuberance with 30° relief angle.

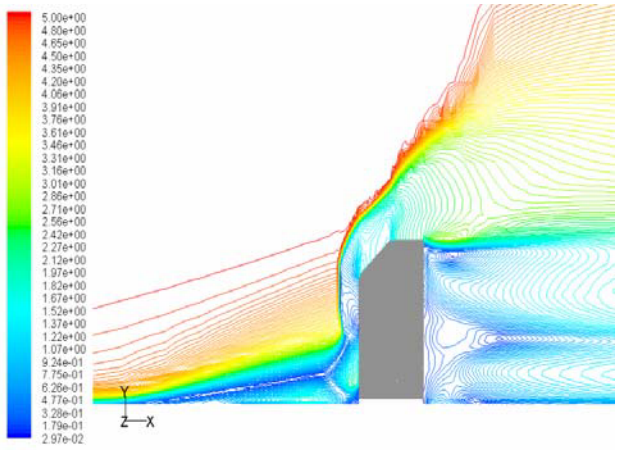

FIG 8: Mach contours for protuberance with 45° relief angle.

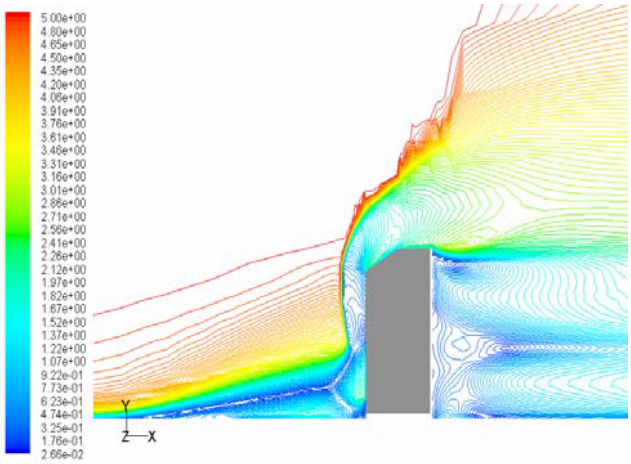

FIG 9: Mach contours for protuberance with 60° relief angle.

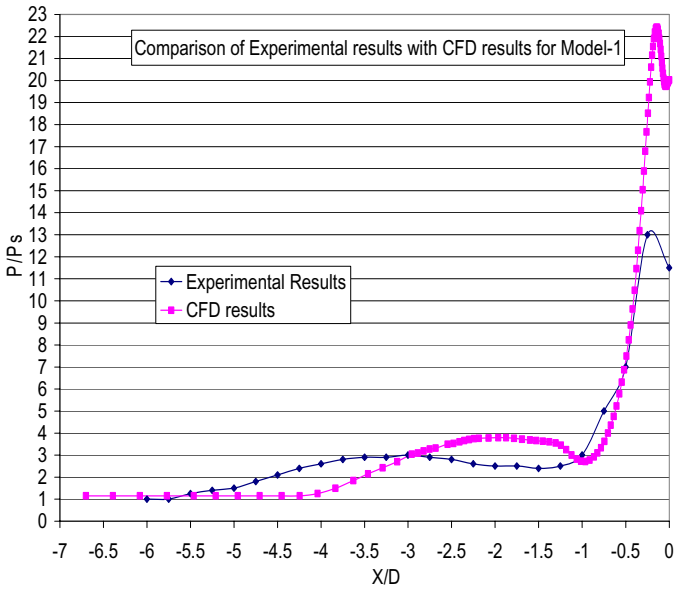

FIG 10: Comparison of CFD results with experimental results for pressure distribution along plate centreline

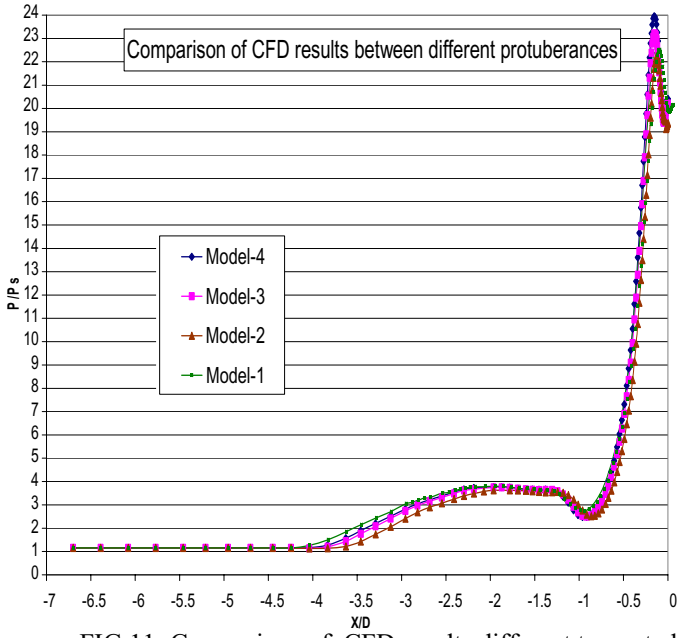

FIG 11: Comparison of CFD results different truncated models with experimental results for pressure distribution along plate centreline

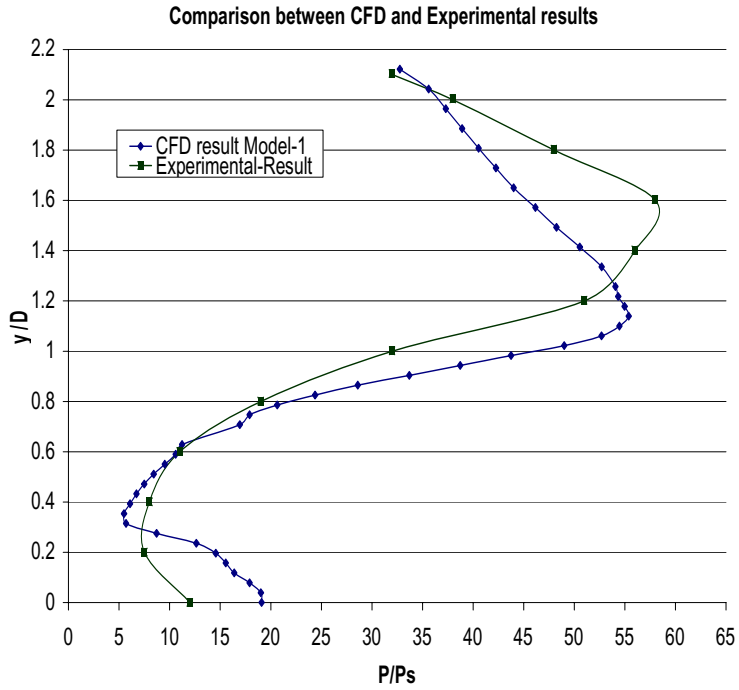

FIG 12: Comparison of CFD results of different truncated models for pressure distribution on windward face

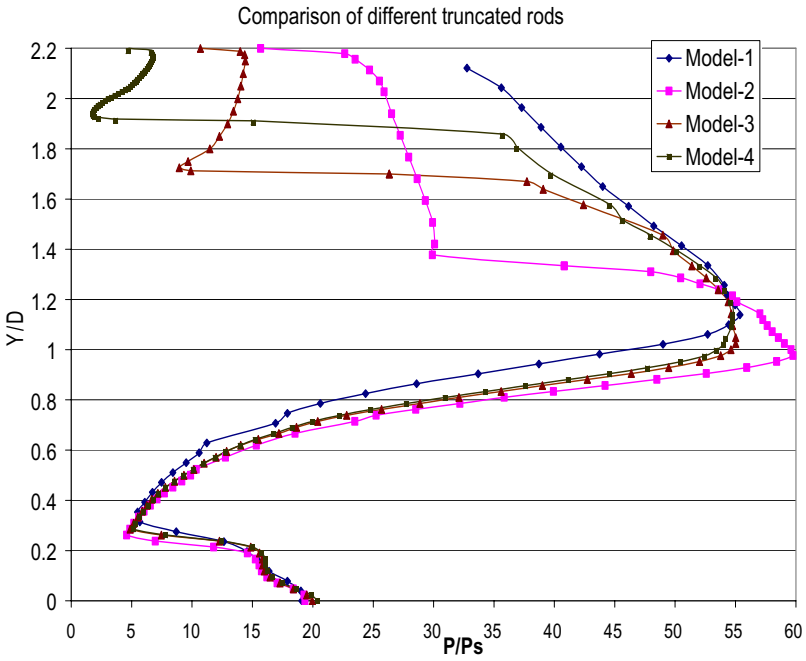

FIG 12: Comparison of CFD results with experimental results for pressure distribution along windward face